

RESEARCH ARTICLE

Experimental Optimization of High-precision Turning Parameters of AL6061 Materials for Automotive Industry Based on Grey Relational Analysis

J. C Puoza^{1*}, T. Zhang², F. Uba³, Y. Kuusana¹, A. Ibrahim¹

¹Faculty of Engineering, Sunyani Technical University, P. O. Box 206, Sunyani, Ghana

²School of Mechanical Engineering, Jiangsu University, Zhenjiang, Jiangsu, 212013, China

³Faculty of Engineering, University of Energy and Natural Resources, P.O. Box 241, Sunyani, Ghana

ABSTRACT - This research article aims to explore the relationship between the machining parameters of a Slant Bed Turning Centre Computer Numerical Control (SB/C/CNC) precision lathe and surface microhardness, dimensional error and surface roughness of AL6061. A technique called the central composite design (CCD) method with 13 experiments was used to evaluate the surface microhardness, dimensional error, and surface roughness after a turning operation using a micro-grooved texture tool. Separate prediction models were developed for each of these characteristics using the response surface method (RSM) in order to find the optimal process parameters for each characteristic. The analysis of variance revealed that the prediction models for surface microhardness, dimensional error, and surface roughness were highly significant, with p-values less than 0.0001. The process parameters that resulted in the highest surface microhardness were a cutting speed (V_c) of 154.363 m/min and a feed rate (f_z) of 0.231 mm/rev. On the other hand, the process parameters that led to the lowest dimensional error and surface roughness were $V_c = 154.363$ m/min, $f_z = 0.1389$ mm/rev, and $V_c = 152.081$ m/min, $f_z = 0.1025$ mm/rev, respectively. The multi-objective prediction model based on gray relational analysis showed an error range of 1.5% to 3.1% and a minimum gray relational degree value of 0.3503 within the feasible process parameter range. The accuracy of this multi-objective prediction model was higher, with a stronger response to the cutting speed V_c compared to the feed rate f_z . The determined feasible process parameter range serves as a useful reference for engineers working with AL6061 materials in turning operations.

ARTICLE HISTORY

Received : 15th June 2023
 Revised : 15th Sept 2023
 Accepted : 06th Dec 2023
 Published : 26th Dec 2023

KEYWORDS

Turning operation
Aluminium-6061 alloy
Machining parameters
Multi-objective optimization
Grey correlation analysis

1.0 INTRODUCTION

An aluminum alloy is a composition consisting mainly of aluminum to which other metals like copper, manganese, silicon, magnesium, and zinc have been added [1]. In the aerospace [2] automotive components construction [3], and engineering industries [4]. aluminum alloy is frequently employed for commercial applications. Other fields where aluminum alloys are used include construction [5, 6], as well as the electrical [7], electromechanical, electronic, and railcar packaging industries. In order to create nanostructures, which require materials with excellent mechanical strength and thermal stability, aluminum alloys are also employed quite successfully. The lightweight and advantageous mechanical and thermal properties of aluminum alloys make them highly significant in the future generation of cars, opening up new possibilities for various applications in the automotive industry [8-10]. There is a wide range of opportunities to utilize aluminum alloys in automotive powertrains, chassis, and body structures [11, 12]. Compared to other metals, aluminum alloy is relatively easy to machine. The minimal energy consumption during the machining of aluminum alloys provides evidence to support this claim [13].

Machinability is a measure of the ease or difficulty with which a material can be machined under a given set of conditions [14]. The machining performance can be determined by multiple factors, including tool life, surface finish, chip evacuation, material removal rate, and power consumption of the machine tools, among others. Therefore, it is crucial to have knowledge of the machinability characteristics of these materials when providing data for researchers and the industry to use [15]. The quest for high efficiency and quality mechanical components drives up competition in the industrial sectors. Optimization methods are applied in this situation to enhance the manufacturing process [16, 17]. Gutema et al. [18] studied the surface roughness and temperature of aluminum 6061 alloy through central composite experimental design for turning and analyzed the influence of different machining parameters on the machined surface quality and temperature. According to the results, the ideal cutting parameters for surface roughness and temperature are 116.37 m/min for the cutting speed, 0.408 mm/rev for the feed rate, 0.538 mm for the cutting depth, and 0.20 mm for the tool nose radius. The corresponding ideal surface roughness and temperature values are 0.374 m and 27.439 °C respectively. Shaik et al. [19] established regression models based on a genetic algorithm, optimized the cutting parameters (axial cutting depth, feed rate and cutting speed) of end-milling, and minimized the tool vibration amplitudes and surface roughness of AL6061 alloy. Using the Taguchi approach and Analysis of Variance (ANOVA), Niranjan et al. [20] optimized the cutting parameters, such as cutting speed, feed rate, and depth of cut, in the turning operation of

aluminum alloy 6061 T6 cylindrical rods. The outcome shown that a better surface finish may be achieved with cutting speeds of 429 m/min, feed rates of 0.05 mm/min, and depths of 1 mm.

The authors of this manuscript made an initial and unique contribution by presenting comparative graphs that highlight the global position of aluminum alloys. These graphs serve as the fundamental basis for the research conducted in this article. The first graph has been created and shows the percentage of the main aluminum alloys utilized in the automotive sector from 2005 to 2023 (Figure 1). Following the study of the graph, we can observe that the majority (32.5%) of Al 6061 alloy is utilized in the automotive sector, followed by Al 2024 at 19.1%, which is our conclusion. These alloys were created by a number of committed businesses with the assistance of major automotive producers to enhance the manufacturing process of diverse aluminum applications. Al 6061 alloy, designed and produced by Universal Alloy Corporation, will be the subject of this investigation. The automotive industry opts for this relatively new aluminum alloy due to its superior characteristics compared to existing aluminum alloys. These advantages include exceptional machinability, favorable formability and bake hardening properties, high strength and toughness, excellent resistance to corrosion, and a remarkable strength-to-weight ratio. [21]. Al 6061 is a versatile material because of all these characteristics.

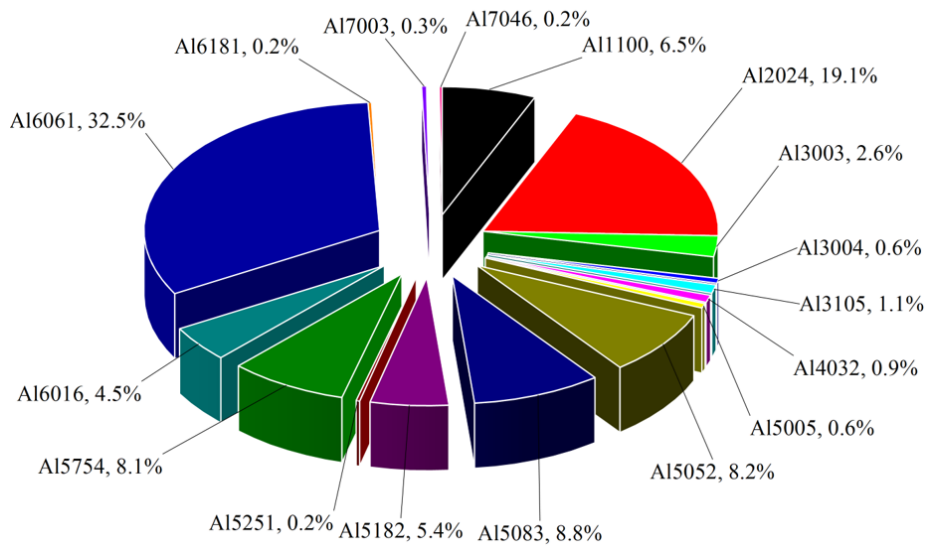


Figure 1. Graph of research work on aluminum alloys usage in the automotive industry for the period, 2005–2023

Another comparative original graph is created by the authors on the machining operations frequency of aluminum alloy as indicated in Figure 2(a). Concerning machining operations, milling (42%) is followed by turning (29%), which is the machining process that has been studied the most on aluminum alloy. The authors have created another distinct comparative graph, as depicted in Figure 2(b), which examines the relationship between the cutting parameters and their influence on surface quality. It is clear from this scenario that the cutting speed with 55% is the most researched parameter, closely followed by the feed rate with 25% and cutting depth with 20%.

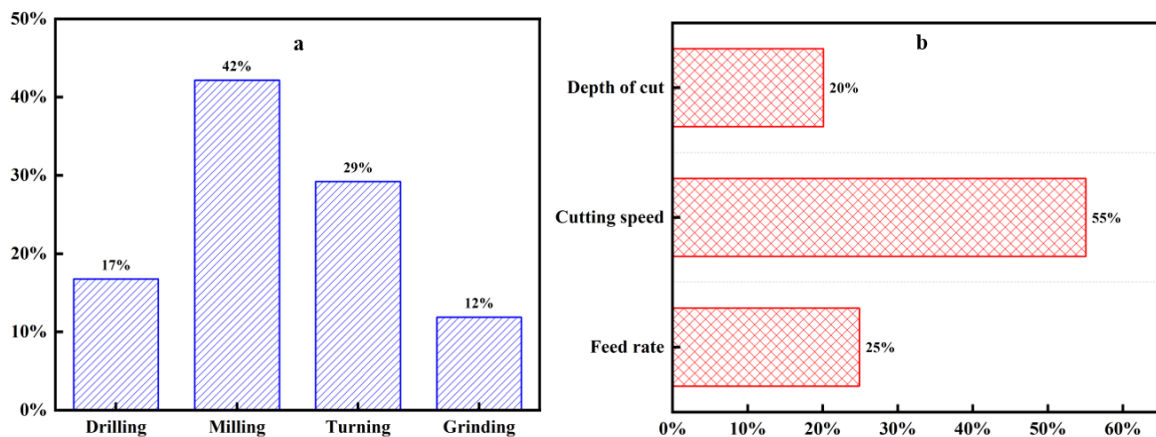


Figure 2. Graph of research work on (a) machining operations and (b) machining parameters on aluminum alloys for the period, 2005–2023

Lastly, Figure 3(a) showcases the research areas that have received the most attention in the study of aluminum alloys, while Figure 3(b) illustrates the mathematical methods employed to optimize the cutting process of these alloys. As per Figure 3(a), the highest proportion, at 18%, is dedicated to the examination of tool wear in aluminum alloy machining. This is closely followed by studies on roughness, deformations, and friction, each accounting for 16% of the research

focus. Hardness, which accounts for 14%, and cutting forces, which accounts for 12% are also very important research directions on aluminum alloy machining. Less research has been done on chip formation and power consumption than has been done on the aforementioned characteristics. Finally, Taguchi and RSM are the most researched mathematical techniques for optimizing the cutting operations for aluminum alloys, according to an analysis of these techniques as elucidated in Figure 3(b). The authors regarded Figures 1 to 3 as highly significant since these graphs were developed using credible and up-to-date research publications. Furthermore, Table 1 provides a concise overview of other research publications that have explored the optimization of AL 6061.

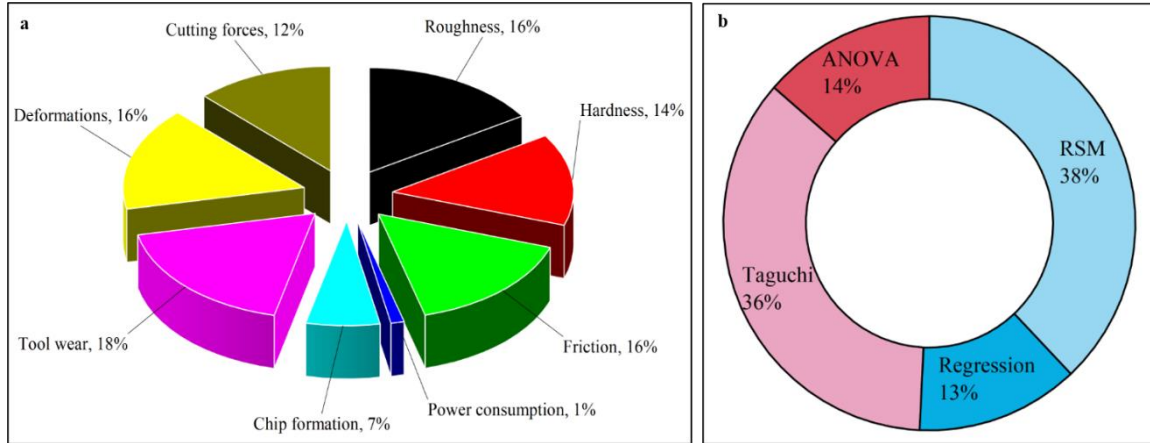


Figure 3. The graph (a) illustrates the research focuses related to the machining of aluminum alloys, while (b) showcases the mathematical techniques utilized to optimize aluminum alloy machining processes from 2005 to 2023

Table 1. The research conducted on machining Al6061 identified and documented

Machining Operation	Aluminum Alloy	Machining Parameters	Brief Overview/Aims	Optimization/Prediction Approach	Author
Milling	Al 6061	Rotational speed, cutting depth, feed rate	Determination of optimum machining parameters influences on surface roughness	Experimental/Taguchi method	[22]
Micro Milling	Al 6061	depth of cut, cutting speed, feed per tooth, number of inserts	In order to decrease the energy consumption per unit and enhance the surface quality	Taguchi method	[23]
Turning	Al 6061	cutting speed, rate of feed, cutting depth, tool nose radius	Identifying the appropriate combination of optimal machining parameters and their interactions to achieve reduced surface roughness and temperature	Response Surface Methodology (RSM) and Analysis of Variance (ANOVA)	[18]
Turning	Al 6061	spindle speed, feed rate, depth of cut	To reduce surface roughness and tool flank wear	Regression analysis, ANOVA	[24]
Turning	Al 6061	cutting speed, rate of feed, cutting depth	optimization of the process parameter on surface roughness produced	Taguchi method	[25]
Turning	Al 6061	cutting speed, rate of feed, cutting depth	To improve on the surface quality of machined components	Response Surface Methodology (RSM) and ANOVA	[26]
End Milling	Al 6061	cutting speed, feed per tooth, cutting depth	Refining the regression equation for surface roughness through optimization	Taguchi and ANOVA	[27]

Numerous studies have been published using aluminum 6061 as the workpiece material using Analysis of Variance (ANOVA) and RSM as indicated by previous scholars in the literature section of this article. However, there is a limited amount of literature available on the utilization of ANOVA, RSM, and GRA for optimizing the input and output parameters in the context of turning aluminum 6061. The GRA application, in particular, offers substantial advantages

for simultaneously optimizing and reducing the number of criteria as well as for bringing about process modifications that improve product quality and productivity. According to engineering practice, the evaluation indexes of surface quality of Al 6061 processing mainly include surface microhardness, dimensional error and surface roughness. These crucial parameters influence surface integrity and are therefore selected as response variables.

In this present study, given the complexity of the experiment and the need for efficient optimization, the researchers opted for the central composite design approach based on the response surface method. This choice aimed to analyze the impact of process parameters on the surface roughness, dimensional error, and surface microhardness during the turning process of Al 6061. Additionally, based on the theory of gray relational analysis, the surface microhardness, dimensional error and surface roughness response characteristics were reduced into a single response index of surface integrity and the optimal machining parameter group and the feasible process parameter domain were determined for turning process of Al 6061 used in the automotive field. The findings presented in this research paper will prove advantageous to various manufacturing industries when making decisions regarding the choice of machine tools, advanced materials, cutting conditions, and cutting tools in real-world engineering applications.

2.0 MATERIALS AND METHODS

The research's materials, laser setup information, surface texture dimensions, the methods utilized to create the textured tool, and the specifics of the semiautomatic lathe machine are all covered in this section.

2.1 Materials

An aluminum alloy AL6061 bar with a diameter of 75 mm and length of 120 mm was selected as the workpiece material. Aluminum alloy AL6061 was selected due to the fact that it has a wide range of applications in the automotive and aerospace industries and the size was based on the commercial availability of the material. Aluminum alloy 6061 is a typical AL-Mg-Si series variable heat-treated strengthening alloy with chemical composition and mechanical properties as mentioned in Table 2 and Table 3 respectively. The YG3X Cemented carbide was selected as the test tool. Carbide-cutting tools have the characteristics of high hardness, high bending strength and high toughness. The YG3X cemented carbide cutting tools have obvious advantages when cutting 6061 aluminum alloy, and can achieve high-efficiency and high-quality processing. The main properties are shown in Table 4.

Table 2. Chemical compositions of AL6061 [18]

Element	Mg	Fe	Si	Zn	Cu	Mn	Ti	Cr
wt%	0.8-1.2	0.7	0.4-0.8	0.25	0.15-0.4	0.15	0.15	0.04-0.35

Table 3. Mechanical properties of the aluminium alloy AL6061 [28]

Method of manufacture	Hardness (HRC)	Tensile strength (MPa)	Yield strength (MPa)	Elongation
Extruded	9.9	308	252	11.2

Table 4. Properties of YG3X cemented carbide [28]

Composition (wt. %)	Density (gcm ⁻³)	Flexural strength (GPa)	Thermal conductivity (W/(m-k))	Thermal expansion coefficient (10 ⁻⁴ /K)
WC + 3%Co	13.8	1.08	87.9	5.3

2.2 Methods

2.2.1 Materials Preparation

In order to ensure the accuracy of the measurement of the textured surface topography, the rake faces of the carbide cutting tools were grounded with 250#, 600#, 800#, 1200#, and 1500# sandpapers respectively. Finally, the W10 was used to polish the tool samples to a surface roughness of about 0.05µm in a metallographic machine.

2.2.2 Surface Texturing

The process of surface texturing involved using an acousto-optic Q-switched diode-pumped Nd:YAG laser micromachining system to texture the rake face of the carbide tool near the main cutting edge. The parameters used were reported by Hua et al. [29]. This system utilized a TEM₀₀ fundamental mode laser beam, and a beam expander telescope device was installed outside the resonator to enhance collimation and focusing capabilities. By directing the laser beam onto the carbide material at its focal point, the material absorbed the energy of the incident laser beam, causing it to heat up until it reached its melting point. As a result, a localized heat-affected zone was created, leading to instantaneous vaporization and ablation of the metal, ultimately resulting in the formation of microgrooves. For the processed surface textures, the slag on the surfaces of the tool sample was treated with metallographic sandpaper. After polishing, the samples were placed in a KYX25-2400L ultrasonic cleaning machine for about 30 minutes. Finally, the samples were

stored in a drying oven before the geometric dimension measurements were performed. The micro-textured groove on the rake face of the tool has a rectangular cross-section. It measures 100 μm in width, with a pitch (distance between adjacent grooves) also measuring 100 μm, and a depth of 50 μm.

2.3 Machining

The turning operations were carried out by a Slant Bed Turning Centre Computer Numerical Control (SB/C/CNC) precision lathe for a cutting length of 80 mm for the machining time of 60 s and a cutting depth of 0.5mm. This lathe has strong rigidity and shock resistance, and the cutting process is very smooth. During the experiment, the carbide tool was clamped on the lathe. The tool's cutting angle parameters are as follows: the rake angle is set at 10°, the rear angle at 8°, the main deflection angle at 45°, and the inclination angle at 0°. The tool has an arc radius of 0.3 mm. To ensure consistent conditions and eliminate the impact of tool wear, each turning experiment was conducted with a fresh cutting edge. Two repetitions were performed for each experiment, and the average value was recorded. Kerosene oil cutting fluid was used as the cutting lubricant in these wet cutting experiments.

The experimental design matrix was created using the Central Composite Design method (CCD) with two factors, cutting speed (V_c) and feed rate (f_z), and five levels. A total of thirteen (13) experiments were generated, consisting of four cube points, five center points, and four axial points. Table 5 provides details of the cutting parameters and their corresponding levels used in this research study. Based on experience, some preliminary experiments were conducted to select the cutting parameters and their levels. The MINITAB software was employed for variance analysis.

Table 5. Machining parameters and their levels used in the turning experiment

S/N	Parameters	Level				
		-1.414	-1	0	1	1.414
1	Feed rate (mm/rev)	103	120	160	200	216
2	Depth of cut (mm)	0.019	0.05	0.125	0.200	0.200

2.3.1 Instrumental Analysis

The surface roughness of the processed specimen was evaluated using a roughness meter (TR2000), as shown in Figure 4(a). Additionally, the surface microhardness of the processed specimen was measured using a hardness tester (TIME5310), as indicated in Figure 4(b). The TIME5310 Portable Hardness tester is a modern digital device designed with advanced microelectronic technology. It offers various features for metal hardness testing, including probe auto recognition, a large memory, USB output, a removable mini-printer, and software. The enhanced display of the tester makes it significantly easier to read the measured values. A digital display micrometer was used to measure the diameter of the processed specimen. In all the measurements, three (3) measurement points were taken equidistantly on the outer surface of the workpiece and each measurement point rotated at 120° in the circumferential direction to obtain three (3) values. The averages of the three sets of values were calculated to obtain the surface roughness, microhardness and the diameter of the specimen respectively. The dimensional error (δ) of the specimen was obtained by Eq (1)

$$\delta = |D_o - D| \tag{1}$$

where δ is the absolute value of the machining error of the test piece, that is, the size error; D is the actual size; D_o is the theoretical size of the workpiece.

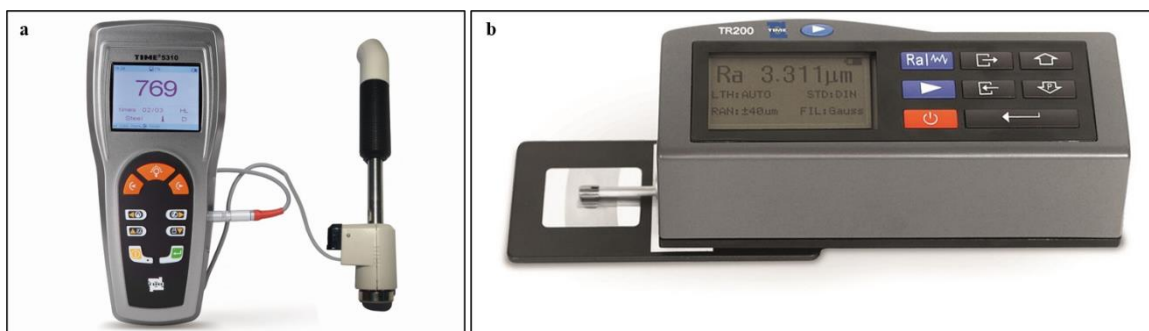


Figure 4. Photograph of (a) TR2000 roughness meter and (b) TIME5310 hardness tester

3.0 RESULTS AND DISCUSSION

The test arrangement and measured results of surface microhardness (H), dimensional error (δ), and surface roughness (Ra) are shown in Table 6.

Table 6. Measured results of experimental work

No.	Machining Input Parameters			Responses	
	V_c (m/mm)	f_z (mm/rev)	H (HB)	\mathcal{D} (mm)	Ra (μm)
1	120	0.050	61.9	0.0240	0.6245
2	103	0.125	64.1	0.0191	0.7225
3	120	0.200	68.4	0.0126	0.7649
4	160	0.019	56.3	0.0274	0.6467
5	160	0.125	58.3	0.0034	0.4568
6	160	0.125	58.5	0.0038	0.4267
7	160	0.125	59.1	0.0055	0.3970
8	160	0.125	58.7	0.0048	0.4071
9	160	0.125	60.1	0.0059	0.4761
10	160	0.231	69.0	0.0192	0.9322
11	200	0.050	51.2	0.0208	0.7224
12	216	0.125	48.2	0.0235	0.9760
13	200	0.200	56.5	0.0221	1.0928

The response surface method is based on the target parameter values solved at each experimental design point, and can quickly give the approximate value of the target parameters at all points in the design space without a complete solution [30]. In this paper, the second-order polynomial response surface of surface roughness, dimensional error and surface microhardness is constructed by using the response surface method and the linear relationship between the surface roughness, dimensional error and surface microhardness and the processing parameters of the SB/C/CNC precision lathe is described respectively. In this research article, the response surface method is used to construct the second-order polynomial of surface roughness, dimensional error and surface microhardness. The linear relationship between surface roughness, dimensional error and surface microhardness and processing parameters of the SB/C/CNC precision lathe is described respectively, and the fitting results are verified by significance. The second-order regression equation of process parameters and response values can be expressed in Eq. (2).

$$\hat{y} = \beta_0 + \sum_{i=1}^n \beta_i x_i + \sum_{i=1}^n \sum_{j=i+1}^n \beta_{ij} x_j + \sum_{i=1}^n \beta_{ii} x_i^2 + \varepsilon \tag{2}$$

In Eq. (2) \hat{y} is the estimated response value; n is the number of process parameters; β is the quadratic regression coefficient; ε is the experimental error.

3.1 Response Surface Model Construction

The measured data of H, δ , and Ra were subjected to regression analysis using MINITAB software. This analysis led to the establishment of a second-order mathematical response model, represented by Eq. (3). The test results, obtained at a predetermined significance level of $F_{0.05}(5,12) = 3.11$, are presented in Table 7. The variance analysis of H was carried out and the model's F value is 83.70 (greater than 3.11), $R_{sq} = 98.35\%$, and $P < 0.0001$, which is less than the confidence coefficient of 0.05. For variance analysis on δ , the F value of the model is 77.93 (greater than 3.11), $R_{sq} = 98.24\%$, and P is less than the confidence coefficient of 0.05. Similarly, the variance analysis of Ra is carried out, and the F value of the model is 129.50 (greater than 3.11), $R_{sq} = 98.93\%$, and $P < 0.0001$, which is much smaller than the confidence coefficient of 0.05. It can be seen that the H, δ , and Ra models have higher reliability and better significance. The columnar comparison between the target real value and the predicted value is shown in Figure 5. It can be clearly seen that the surface microhardness, dimensional error and surface roughness are well-fitted to the mathematical order response model of the lathe processing parameters.

Table 7. Variance analysis

Object	Source	Degree of freedom	Sum of squares	Mean square	F	P	% Contribution
H	Model	5	408.185	81.637	83.70	0.000	98.35

Linear	2	363.908	181.685	186.27	0.000	87.69	
V_c	1	253.211	252.486	258.85	0.000	61.01	
f_z	1	110.697	110.885	113.68	0.000	26.67	
Square	2	43.917	21.958	22.51	0.001	10.58	
V_c^2	1	19.071	13.576	13.92	0.007	4.60	
f_z^2	1	24.846	24.846	25.47	0.001	5.99	
2-Way	1	0.360	0.360	0.37	0.563	0.09	
$V_c \times f_z$	1	0.360	0.360	0.37	0.563	0.09	
Error	7	6.828	0.975			1.65	
Total	12	415.012				100.00	
Model summary		$R_{sq} = 98.35\%$	$R_{sq} (adj) = 97.18\%$				
δ	Model	5	0.000951	0.000190	77.93	0.000	98.24
	Linear	2	0.000078	0.000039	15.93	0.002	8.05
	V_c	1	0.000019	0.000017	7.04	0.033	1.97
	f_z	1	0.000059	0.000061	24.82	0.002	6.08
	Square	2	0.000832	0.000416	170.59	0.000	86.02
	V_c^2	1	0.000306	0.000413	169.33	0.000	31.65
	f_z^2	1	0.000526	0.000526	215.63	0.000	54.36
	2-Way	1	0.000040	0.000040	16.53	0.005	4.17
	$V_c \times f_z$	1	0.000040	0.000040	16.53	0.005	4.17
	Error	7	0.000017	0.000002			1.76
	Total	12	0.000968				100.00
	Model summary		$R_{sq} = 98.24\%$	$R_{sq} (adj) = 96.97\%$			
R_a	Model	5	0.636953	0.127391	129.50	0.000	98.93
	Linear	2	0.180556	0.088053	89.51	0.000	28.04
	V_c	1	0.075996	0.072888	74.09	0.000	11.80
	f_z	1	0.104560	0.103217	104.92	0.000	16.24
	Square	2	0.443173	0.221586	225.25	0.000	68.83
	V_c^2	1	0.233660	0.290083	294.88	0.000	36.29
	f_z^2	1	0.209513	0.209513	212.98	0.000	32.54
	2-Way	1	0.013225	0.013225	13.44	0.008	2.05
	$V_c \times f_z$	1	0.013225	0.013225	13.44	0.008	2.05
	Error	7	0.006886	0.000984			1.07
	Total	12	0.643840				100.00
	Model summary		$R_{sq} = 98.93\%$	$R_{sq} (adj) = 98.17\%$			

$$\begin{cases} H = 56.23 + 0.1510V_c - 18.5f_z - 0.000875V_c^2 + 336.3f_z^2 - 0.100V_c * f_z \\ \delta = 0.1714 - 0.001635V_c - 0.5923f_z + 0.000005V_c^2 + 1.547f_z^2 + 0.001058V_c * f_z \\ R_a = 3.978 - 0.04079V_c - 9.26f_z + 0.000128V_c^2 + 30.88f_z^2 + 0.01917V_c * f_z \end{cases} \quad (3)$$

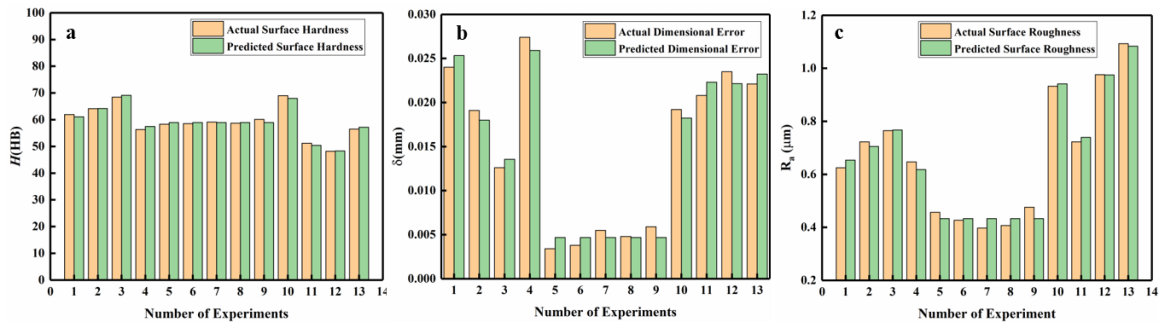


Figure 5. Comparison histograms of (a) actual surface hardness value and predicted value, (b) actual dimensional error value and predicted value (c) actual surface roughness value and predicted value

In Eq. (3) V_c is the cutting speed, m/min; f_z is the feed rate, mm/rev; H represents the predicted surface microhardness, HB; δ represents the predicted dimensional error, mm; R_a represents the predicted surface roughness, μm .

3.2 Analysis of Influence Law

Figure 6 displays the main effect of surface microhardness (H) and process parameters. In Figure 6(a), the relationship between cutting speed and the surface microhardness of the processed AL6061 is shown. It can be observed that as the cutting speed increases from 103 m/min to 216 m/min, the surface microhardness gradually decreases. This decrease can be attributed to the generation of more cutting heat as the speed increases, leading to a softening of the workpiece surface. Additionally, the shortened contact time between the AL6061 rod and the cutting edge prevents the surface work hardening process from fully completing, resulting in a reduction in surface microhardness. In Figure 6(b), the response trend of surface microhardness to the feed rate is depicted. It indicates that the surface microhardness increases with an increase in the feed rate. As the lathe's feed rate increases, the friction between the AL6061 workpiece surface and the cutting tool intensifies. This intensification leads to plastic deformation on the surface, causing the entanglement of dislocations within the crystal lattice. Consequently, the grains elongate, break, and form a fibrous structure, resulting in the phenomenon of hardening. This hardening process promotes an increase in the surface microhardness of the workpiece.

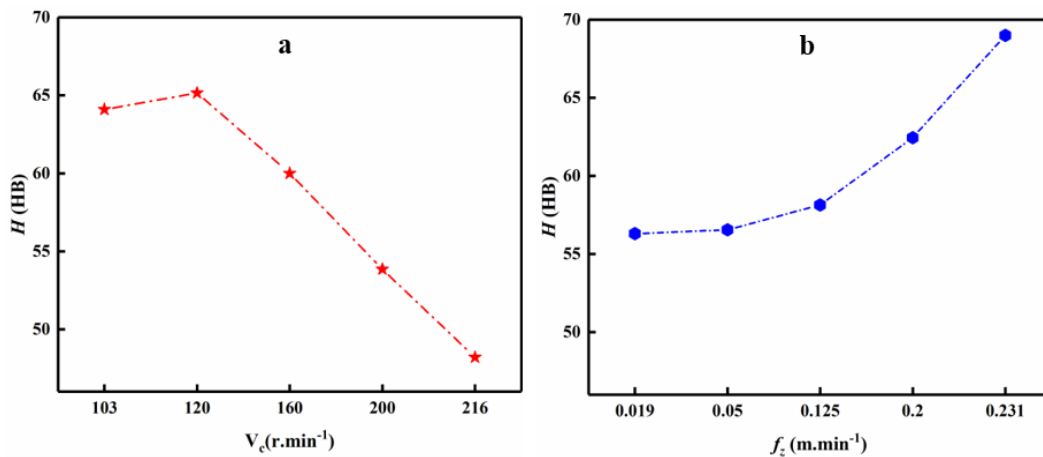


Figure 6. Main effect plot of surface microhardness with (a) cutting speed and (b) feed rate

The main effect of dimensional error and process parameters is shown in Figure 7. The response trend of the dimensional error to the cutting speed is shown in Figure 7(a). With the increase in the cutting speed, the dimensional error shows a trend of decreasing first and then increasing. The response trend of the dimensional error to the feed rate is shown in Figure 7(b). When the feed rate is adjusted from 0.019 mm/rev to 0.125 mm/rev, there is a significant decrease in dimensional error. However, when the feed rate is further increased from 0.125 mm/rev to 0.231 mm/rev, the dimensional error gradually starts to increase. The overall dimensional error is less than 0.03 mm, and the overall change amplitude is small, which further indicates that the SB/C/CNC lathe has higher machining accuracy.

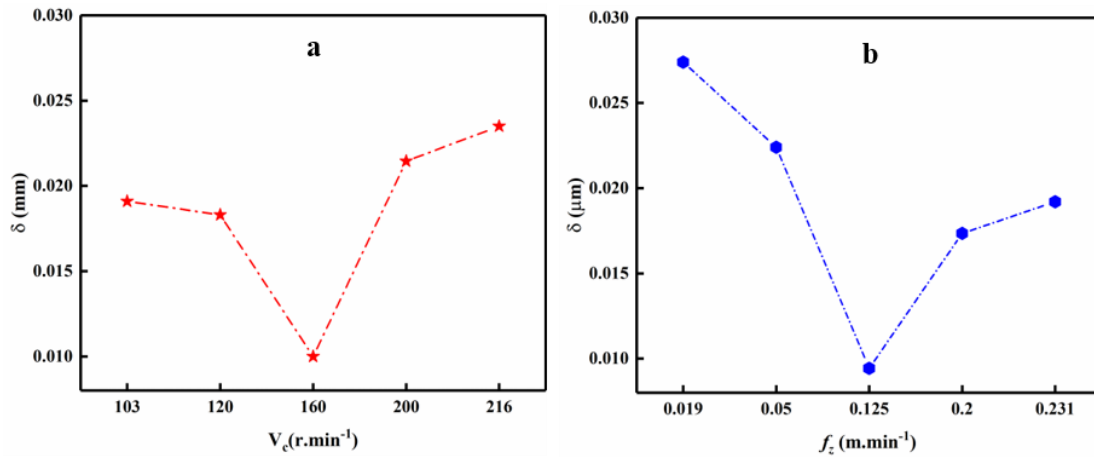


Figure 7. Main effect plots of dimensional error with (a) cutting speed and (b) feed rate

Figure 8 illustrates the main effect of surface roughness and process parameters. In Figure 8(a), the relationship between cutting speed and the surface roughness of the processed AL6061 is depicted. When the cutting speed ranges from 103 m/min to 160 m/min, the surface roughness demonstrates a gradual decrease. However, when the cutting speed increases from 160 m/min to 216 m/min, the surface roughness rapidly increases. The gradual increase in cutting heat transmitted by the tool as the cutting speed rises from 103 m/min to 160 m/min leads to visible high-frequency vibrations in the test material. Consequently, the surface roughness of the workpiece experiences a sharp increase. Figure 8(b) showcases the response trend of surface roughness to the feed rate. At low feed rates, the prolonged presence of cutting heat on the cutting surface of the workpiece results in the formation of a built-up edge on the cutting tool. This, in turn, causes regular lines to appear on the surface of the AL6061 material, leading to poor surface quality. As the feed rate gradually increases within the range of 0.125-0.231 mm/rev, the accelerated contact wear between the cutting edge and the AL6061 material generates a significant amount of cutting heat, causing the surface roughness to sharply increase. The overall trend aligns closely with the variation observed in dimensional error.

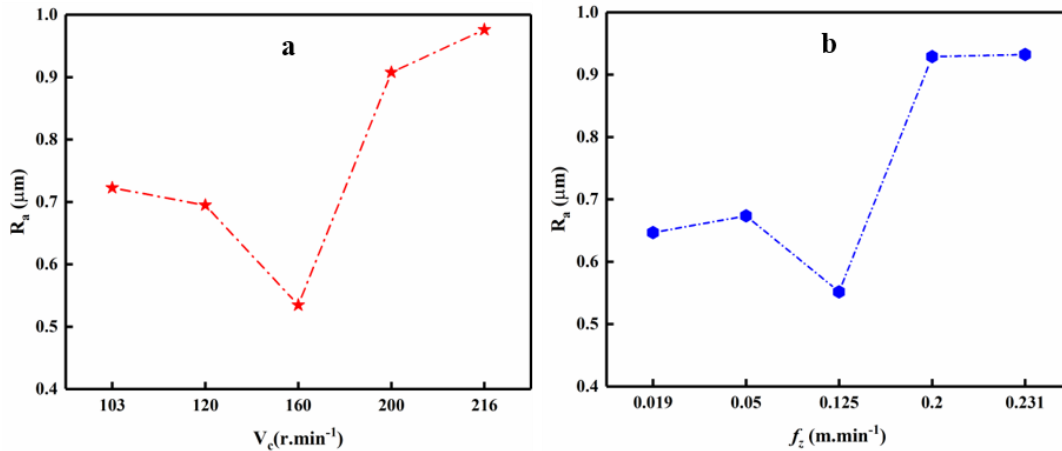


Figure 8. Main effect plots of surface roughness with (a) cutting speed and (b) feed rate

Based on the second-order mathematical prediction model for each response, an interaction diagram of the cutting process parameters is presented in Figure 9. In Figure 9(a), it is evident that a higher surface microhardness can be achieved with a lower cutting speed and a higher feed rate. The influence of the spindle speed and feed rate on dimensional error is relatively similar, as depicted in Figure 9(b). When cutting AL6061 material using an SB/C/CNC lathe, changes in cutting speed have a more significant impact on surface roughness, and an increase in cutting speed leads to relatively larger changes in surface roughness. Figure 9 reveals that the maximum surface microhardness (H_{max}) is 73.80HB, with corresponding process parameters of cutting speed (V_c) at 154.363 m/min and feed rate (f_z) at 0.231 mm/rev. The minimum dimensional error is 0.004315 mm, with corresponding process parameters of cutting speed (V_c) at 154.363 m/min and feed rate (f_z) at 0.1389 mm/rev. The minimum surface roughness ($R_{a_{min}}$) is 0.4055 μm, with corresponding process parameters of cutting speed (V_c) at 152.081 m/min and feed rate (f_z) at 0.1025 mm/rev.

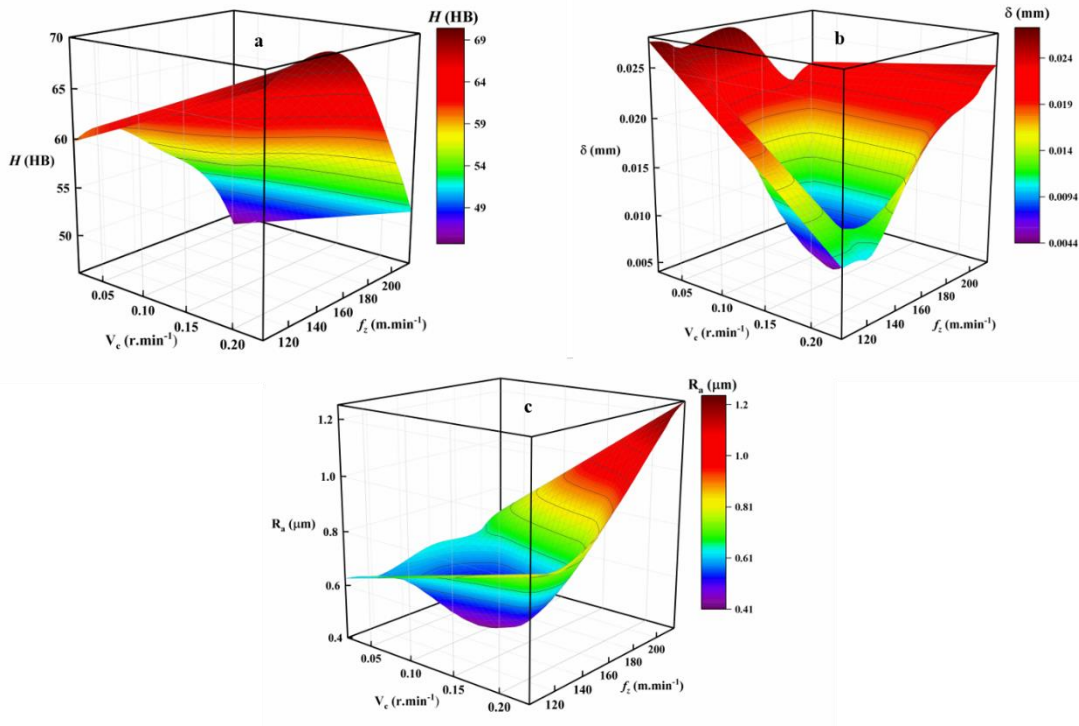


Figure 9. 3D response surface due to interaction of cutting speed and feed rate on (a) surface hardness, (b) dimensional error and (c) surface roughness

3.3 Multi-Objective Optimization Model Construction

3.3.1 Gray Relational Degree Calculation Process

Gray Relational Analysis (GRA) is utilized in multi-objective optimization research to transform multiple optimization objectives into gray relational degree values. This conversion process involves dimensionality reduction techniques. Once the objectives are converted, single-objective optimization analysis is performed on them. The significance of the gray correlation degree lies in its value, where a higher value indicates a stronger correlation and, consequently, a more favorable input response.

- a) Normalization processing. Normalize the surface roughness, dimensional error, and surface microhardness to [0, 1] respectively. The smaller the surface roughness and dimensional error, the better. The data transformation is shown in Eq. (4); The greater the microhardness, the better, and its data transformation is shown in Eq. (5).

$$\eta = \frac{\max(y) - y}{\max(y) - \min(y)} \tag{4}$$

$$\eta = \frac{y - \min(y)}{\max(y) - \min(y)} \tag{5}$$

In Eqs. (4) and (5): η is the corresponding normalized value obtained from the test; "max(y)" represents the highest value of the actual response, while "min(y)" represents the lowest value of the actual response. In this context, "y" refers to the actual value for each set of process parameters.

- b) Gray Relational Coefficient (G_{RC}) computation. The Gray Relational Coefficient (G_{RC}) is computed to assess the correlation between the measurement results and the optimal solution. The comparison sequence of the data being analyzed is represented by η . The calculation of G_{RC} is demonstrated in Eqs. (6)-(7).

$$G_{RC} = \frac{\Delta_{\min} + \xi \Delta_{\min}}{\Delta + \xi \Delta_{\max}} \tag{6}$$

$$\Delta = 1 - \eta \tag{7}$$

In Eq. (7) Δ represents the deviation sequence; Δ_{\min} and Δ_{\max} are the minimum and maximum values of the deviation sequence; ξ is the judgment coefficient, $\xi \in [0, 1]$, ξ is taken as 0.5 here.

- c) Gray Relational Grade (G_{RG}) Calculation. The Gray Relational Grade (GRG) is computed to assess the correlation between the experimental process parameters and the response. It represents the weighted sum of the Gray Relational Coefficient (G_{RC}). A higher G_{RG} indicates a closer match between the corresponding process parameter combination and the expected value. The calculation of G_{RG} is demonstrated in Eq. (8)

$$G_{RG} = \sum_{i=1}^n \beta_i G_{RC} \tag{8}$$

In Eq. (8) β_i is the weight of the i^{th} response variable, which is obtained from step 4 through the analytic hierarchy

$$\sum_{i=1}^n \beta_i = 1$$

process,

- d) Analytic Hierarchy Process (AHP). In practical applications, the reference and importance of each response are not average. To ensure that the weights of each response are consistent with the actual application requirements, the AHP is used to determine the corresponding weights of each response in G_{RG} calculation. By constructing the response evaluation matrix P, the nine-level scaling method is used to make quantitative comparisons between different responses. Label according to the following basic principles: "1" indicates that the two targets have the same importance; "2-9", the larger the number, the higher the importance; among them, the importance of the i^{th} response relative to the j^{th} response is a_{ij} , then the importance of the j^{th} response relative to the i^{th} response is $a_{ij} = 1/a_{ji}$. Using the scoring method of production experts and research experts, construct a response evaluation matrix P, as shown in Eq. (9). By finding the eigenvector x corresponding to the largest eigenvalue λ_{\max} of the matrix P, the response weight matrix β is obtained after normalization.

$$P = [a_{ij}]_{n \times n} = \begin{bmatrix} a_{11} & \dots & a_{1n} \\ \vdots & & \vdots \\ a_{n1} & \dots & a_{nn} \end{bmatrix} \tag{9}$$

3.3.2 Gray Relational Degree Calculation Results and Analysis

The test results were normalized using Eqs. (4)-(5), and the G_{RC} value was calculated using Eq. (6). Afterwards, the Analytic Hierarchy Process (AHP) was employed to construct the response matrix P, as illustrated in Eq. (10). The maximum eigenvalue λ_{\max} was determined to be 3.0658, and its corresponding eigenvectors were presented in Eq. (11). The weight matrix β was obtained through normalization, as depicted in Eq. (12). Notably, the weight assigned to surface roughness is 0.7235, the weight for dimensional error is 0.1932, and the weight for microhardness is 0.0833. These weights indicate the primary evaluation factors for the turning operation. Finally, these values were substituted into Eq. (8) to calculate G_{RG} . The computation results are presented in Table 8 and Table 9.

$$P = \begin{bmatrix} 1 & 5 & 7 \\ 1/5 & 1 & 3 \\ 1/7 & 1/3 & 1 \end{bmatrix} \tag{10}$$

$$x = (9.0246 \quad 2.3270 \quad 1.0000)^T \tag{11}$$

$$\beta = (0.7235 \quad 0.1932 \quad 0.0833)^T \tag{12}$$

Table 8. Normalization and calculated deviation of responses

Exp. No.	Normalization			Deviation		
	$\eta(H)$	$\eta(\delta)$	$\eta(R_a)$	$\Delta(H)$	$\Delta(\delta)$	$\Delta(R_a)$
1	0.659	0.659	0.142	0.341	0.858	0.327
2	0.764	0.764	0.346	0.236	0.654	0.468
3	0.971	0.971	0.617	0.029	0.383	0.529
4	0.389	0.389	0.000	0.611	1.000	0.359
5	0.486	0.486	1.000	0.514	0.000	0.086

6	0.495	0.495	0.983	0.505	0.017	0.043
---	-------	-------	-------	-------	-------	-------

Table 8. (Cont.)

Exp. No.	Normalization			Deviation		
	$\eta(H)$	$\eta(\delta)$	$\eta(R_a)$	$\Delta(H)$	$\Delta(\delta)$	$\Delta(R_a)$
7	0.524	0.524	0.913	0.476	0.087	0.000
8	0.505	0.505	0.942	0.495	0.058	0.015
9	0.572	0.572	0.896	0.428	0.104	0.114
10	1.000	1.000	0.342	0.000	0.658	0.769
11	0.144	0.144	0.275	0.856	0.725	0.468
12	0.000	0.000	0.163	1.000	0.838	0.832
13	0.399	0.399	0.221	0.601	0.779	1.000

Table 9. Calculated G_{RC} and G_{RG} and the corresponding ranking of G_{RG}

Exp. No.	Grey Relational Coefficient			Grade	Ranking
	$G_{RC}(H)$	$G_{RC}(\delta)$	$G_{RC}(R_a)$	G_{RC}	
1	0.594	0.368	0.605	0.558	6
2	0.680	0.433	0.517	0.514	9
3	0.945	0.566	0.486	0.540	7
4	0.450	0.333	0.582	0.523	8
5	0.493	1.000	0.853	0.852	4
6	0.498	0.968	0.921	0.895	3
7	0.512	0.851	1.000	0.931	1
8	0.502	0.896	0.972	0.918	2
9	0.539	0.828	0.815	0.794	5
10	1.000	0.432	0.394	0.452	11
11	0.369	0.408	0.517	0.483	10
12	0.333	0.374	0.375	0.372	12
13	0.454	0.391	0.333	0.355	13

Table 10 demonstrates that a higher gray correlation degree indicates a better target response for the corresponding test process parameter combination. By analyzing the average gray correlation degree for five levels of cutting speed (V_c) and feed rate (f_z), it can be determined that the optimal level for V_c is Level 3 (160 m/min), and the optimal level for f_z is Level 3 (0.125 mm/rev). Additionally, based on range analysis theory, it is observed that the cutting speed has a greater impact on the multi-target response compared to the feed rate, as indicated by the max-min values.

Table 10. Average value of each grey correlation degree under different process parameters

Process Parameters	V_c (m.mm ⁻¹)	f_z (mm.rev ⁻¹)
Level 1	0.514102	0.523097
Level 2	0.548911	0.520741
Level 3	0.766325	0.753587
Level 4	0.418966	0.447136
Level 5	0.371547	0.451721
Max–Min	0.394778	0.306451

After the single-objective analysis of each response, it can be found that the microhardness, dimensional error and surface roughness are all parameter-dependent responses, so the gray relational degree G_{RG} is also a parameter-dependent response. It is evident that the impact of process parameters on the gray correlation degree can be expressed as a weighted sum of the influences of surface microhardness, dimensional error, and surface roughness. The impact of process parameters on the three can be reflected by the change in the gray correlation degree, and the multi-objective prediction of microhardness, dimensional error and surface roughness can be realized by predicting the gray correlation degree.

3.3.3 G_{RG} Response Model Construction

Equation (13) presents the second-order mathematical prediction model for G_{RG} . The results of variance analysis and residual analysis for the second-order mathematical prediction model of gray relational degree G_{RG} are displayed in Table 11. The given significance level is $F_{0.05}(5,12) = 3.11$. ANOVA was performed on G_{RG} , and the F value of the model was 55.69 (greater than 3.11), $R_{sq} = 97.54\%$, and $P < 0.0001$, far less than the confidence coefficient of 0.05. At the same time, R_{sq} is very close to $R_{sq}(adj)$, indicating that the reliability of the prediction model is high. The distribution and comparison between the predicted value of the model and the real value are shown in Figure 10. There is no significant difference between the predicted value and the real value, the error range is 1.5% - 3.1%, and there are no abnormal points, which shows that the prediction model fits the observed value well.

$$G_{RG} = -2.958 + 0.04234 V_c + 9.53 f_z - 0.000133 V_c^2 - 33.87 f_z^2 - 0.00922 V_c * f_z \quad (13)$$

Table 11. Variance analysis of G_{RG} response model

Object	Source	Degree of freedom	Sum of squares	Mean square	F	P
G_{RG}	Model	5	0.540158	0.108032	55.64	< 0.0001
	Error	7	0.013591	0.001942		
	Total	12	0.553749			
Model summary			$R_{sq} = 97.54\%$	$R_{sq}(adj) = 97.32\%$		

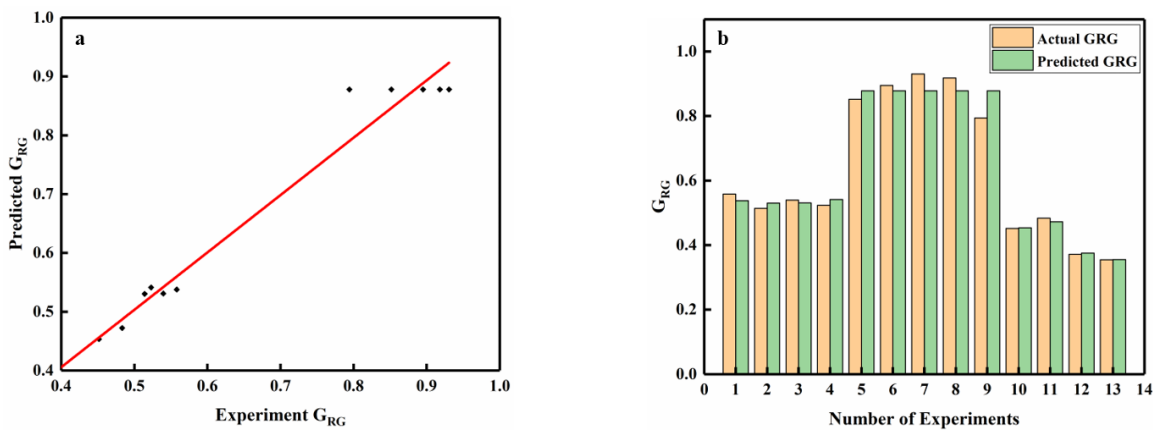


Figure 10. Graph of G_{RG} (a) distribution of predicted value and real value (b) comparison of predicted value and real value

Using the response optimizer in the MINITAB software combined with the response surface (Figure 11) to optimize the analysis of the G_{RG} response surface prediction model, the optimal gray correlation degree $G_{RG_{max}}$ obtained by the response surface method is 0.8832, and the corresponding process parameter group is: Cutting speed $V_c = 154.363$ m/min, feed rate $f_z = 0.1196$ mm/rev.

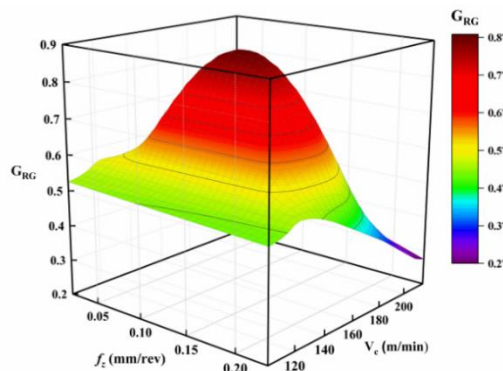


Figure 11. Response surface of G_{RG} process parameters

3.3.4 Test Verification

By analyzing the test results, the optimal gray relational degree $G_{RG_{max}}$ process parameter group is determined, and the $G_{RG_{max}}$ is verified through the experiments below. In order to compare with the $G_{RG_{max}}$ process parameter group in the design test run, the maximum surface microhardness H_{max} , the minimum dimensional error δ_{min} , the minimum surface roughness Ra_{min} , and the optimal gray correlation degree process parameter group were selected as the control experiment. A comparison of test results is shown in Table 12. From the result, the surface microhardness obtained by the H_{max} process parameter group is the highest. However, the dimensional error and the surface roughness values obtained by the δ_{min} and Ra_{min} process parameter group respectively, are relatively the lowest. This result proves the feasibility of the single-objective prediction model of surface microhardness, dimensional error and surface roughness.

In the test results obtained by the $G_{RG_{max}}$ process parameter group compared with the Ra_{min} process parameter group, the dimensional error is reduced by about 34.48%, and the surface microhardness is increased by about 5.50%. Similarly, comparing the $G_{RG_{max}}$ process parameter group with the δ_{min} process parameter group, the surface roughness is reduced. However, when you compare the result of $G_{RG_{max}}$ process parameter group with the H_{max} process parameter group, the surface microhardness increased by about 12.56% and the surface roughness decreased by about 54.38%. This further proves the feasibility of the response surface method based on gray relational analysis.

To verify the applicability of the $G_{RG_{max}}$ process parameter group to the machining of different sizes of AL6061 material, the AL6061 shaft with $\phi = 6\text{mm}$ was selected for experimental verification. The test results show that $Ra = 0.490 \mu\text{m}$, $\delta = 0.0088 \text{ mm}$, and $H = 62.9\text{HB}$. The test results meet the process requirements and verify the applicability of the optimized process parameters to different sizes of shafts.

Table 12. Experimental response optimal process parameter group

Object	Parameter	V_c (m/min)	f_z (mm/rev)	H ((HB)	δ (mm)	Ra (μm)
H_{max}	Prediction	103.0	0.2310			
	Actual	103	0.231	70.8	0.0187	0.912
δ_{min}	Prediction	154.3636	0.1389			
	Actual	154	0.139	62.7	0.0039	0.457
Ra_{min}	Prediction	152.0808	0.1025			
	Actual	152	0.102	58.5	0.0116	0.396
$G_{RG_{max}}$	Prediction	154.3636	0.1196			
	Actual	154	0.120	61.9	0.0076	0.416

3.3.5 Feasible Process Parameter Domains

Based on the multi-objective optimization outcomes for process parameters and the resulting surface microhardness, dimensional error, and surface roughness, a contour map is generated, as depicted in Figure 12.

In engineering applications, the maximum threshold for surface roughness is $0.8 \mu\text{m}$, the maximum threshold for dimensional error is 0.05 mm , and the minimum threshold for surface microhardness is 50HB for AL6061 alloy. At these thresholds, the corresponding minimum evaluation index of $G_{RG_{max}}$ is determined to be 0.3503 . By solving the isocline boundary value and identifying the gradient direction associated with the minimum evaluation index of G_{RG} in Figure 12, the parameter interval of the feasible process parameter domain can be determined. This information serves as a valuable reference for engineering practice.

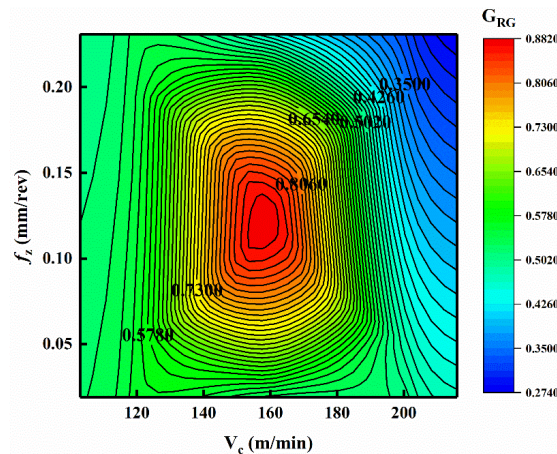


Figure 12. Contour map of G_{RG} process parameters

4.0 CONCLUSIONS

In this study, laser surface texturing technology was utilized to create micro-groove textures on the rake surface of a YG3X cemented carbide cutting tool. Subsequently, multiple-factor turning experiments were conducted on an SB/C/CNC precision lathe using Al 6061 as the workpiece material. Based on the test data, a single-objective response model for microhardness, dimensional error, and surface roughness was constructed using the response surface method. To optimize the surface quality, multi-objective optimization was performed using gray relational theory to reduce the dimensionality of the optimization target. The following conclusions were drawn from the research:

- The analysis of surface roughness and dimensional error revealed an initial decreasing trend followed by an increase with the increase in process parameters such as cutting speed and feed rate. However, surface microhardness exhibited an increasing trend with the increase in cutting speed. Additionally, surface microhardness showed a gradual decrease and subsequent increase with the increase in feed rate.
- The process parameter combination with the highest surface microhardness was found to be $V_c = 154.363$ m/min and feed rate $f_z = 0.231$ mm/rev. On the other hand, the process parameter combinations resulting in the lowest dimensional error and surface roughness were $V_c = 154.363$ m/min, feed rate $f_z = 0.1389$ mm/rev and $V_c = 152.081$ m/min, feed rate $f_z = 0.1025$ mm/rev, respectively.
- Experimental verification confirmed the consistency between the predicted and experimental values. Moreover, the optimized process parameters effectively improved surface microhardness, dimensional error, and surface roughness, indicating that the combination of optimized process parameters for each target can lead to better overall performance during the turning of Al 6061.
- The lowest evaluation index $G_{RG_{max}}$ of the gray correlation value for surface microhardness, dimensional error, and surface roughness was found to be 0.3503. This finding holds practical significance for the machining of Al 6061 rods in real-world engineering scenarios.
- In conclusion, the findings of this research paper offer valuable insights for machining science practice from various perspectives. The authors recommend further research on the selection of machining parameters, machine tools, cutting tools, and advanced materials to provide additional guidance for the manufacturing of machine parts.

5.0 CONFLICT OF INTEREST

The authors state that they do not have any conflicting financial interests or personal relationships that could have influenced the work presented in this paper.

6.0 ACKNOWLEDGMENT

This research work has not received any financial support from any research grant.

7.0 REFERENCES

- N. Sharma, G. Saini, S. Goyal, and P. Sharma, "A comprehensive study on aluminium alloy series – a review," *Recent Advances in Mechanical Engineering*, vol. 1, pp. 11-27, 2017.
- R. Montanari, A. Palombi, M. Richetta, and A. Varone, "Additive Manufacturing of Aluminum Alloys for Aeronautic Applications: Advantages and Problems," *Metals*, vol. 13, no. 4, p. 716, 2023.
- A. Graf, "Chapter 3 - Aluminum alloys for lightweight automotive structures," in *Materials, Design and Manufacturing for Lightweight Vehicles (Second Edition)*, P. K. Mallick Ed.: Woodhead Publishing, 2021, pp. 97-123.

- [4] B. Stojanovic, M. Bukvic, and I. Epler, "Application of aluminum and aluminum alloys in engineering," *Applied engineering letters: Journal of Engineering and Applied Sciences*, vol. 3, no. 2, pp. 52-62, 2018.
- [5] Z. Wang, M. Li, Q. Han, X. Yun, K. Zhou, L. Gardner, and F. M. Mazzolani, "Structural fire behaviour of aluminium alloy structures: Review and outlook," *Engineering Structures*, vol. 268, p. 114746, 2022.
- [6] E. Georgantzia, M. Gkantou, and G. S. Kamaris, "Aluminium alloys as structural material: A review of research," *Engineering Structures*, vol. 227, p. 111372, 2021.
- [7] H. S. Abdo, A. H. Seikh, J. A. Mohammed, and M. S. Soliman, "Alloying Elements Effects on Electrical Conductivity and Mechanical Properties of Newly Fabricated Al Based Alloys Produced by Conventional Casting Process," (in eng), *Materials (Basel)*, vol. 14, no. 14, 2021.
- [8] D. Varshney and K. Kumar, "Application and use of different aluminium alloys with respect to workability, strength and welding parameter optimization," *Ain Shams Engineering Journal*, vol. 12, no. 1, pp. 1143-1152, 2021.
- [9] A. O. Emmanuel, O. S. I. Fayomi, and I. G. Akande, "Aluminium Alloys as Advanced Materials: A short communication," *IOP Conference Series: Materials Science and Engineering*, vol. 1107, no. 1, p. 012024, 2021.
- [10] M. K. Gupta, P. Niesłony, M. Sarikaya, M. E. Korkmaz, M. Kuntoğlu, and G. M. Królczyk, "Studies on Geometrical Features of Tool Wear and Other Important Machining Characteristics in Sustainable Turning of Aluminium Alloys," *International Journal of Precision Engineering and Manufacturing-Green Technology*, vol. 10, pp. 1393-1406, 2023.
- [11] J. Stroh, D. Sediako, and D. Weiss, "The Effects of Iron-Bearing Intermetallics on the Fitness-for-Service Performance of a Rare-Earth-Modified A356 Alloy for Next Generation Automotive Powertrains," *Metals*, vol. 11, no. 5, p. 788, 2021.
- [12] W. Zhang and J. Xu, "Advanced lightweight materials for Automobiles: A review," *Materials & Design*, vol. 221, p. 110994, 2022.
- [13] L. Troeger and E. Starke Jr, "Microstructural and mechanical characterization of a superplastic 6xxx aluminum alloy," *Materials Science and Engineering: A*, vol. 277, no. 1-2, pp. 102-113, 2000.
- [14] A. U. Samuel, A. O. Araoyinbo, R. R. Elewa, and M. B. Biodun, "Effect of Machining of Aluminium Alloys with Emphasis on Aluminium 6061 Alloy – A Review," *IOP Conference Series: Materials Science and Engineering*, vol. 1107, no. 1, p. 012157, 2021.
- [15] J. C. Puoza, S. T. Appiah, T. Zhang, and B. Aboagye, "Chamfer drill geometric parameters optimisation by finite element simulation and experimental analysis," *International Journal of Machining and Machinability of Materials*, vol. 22, no. 5, pp. 406-429, 2020.
- [16] S. Srinivasan, S. Thirumurugaveerakumar, N. Nagarajan, N. Mohammed Raffic, and K. Ganesh Babu, "A review of optimization techniques in machining of composite materials," *Materials Today: Proceedings*, vol. 47, pp. 6811-6814, 2021.
- [17] D. Jaurker, M. K. Pradhan, S. Jaurker, and R. Malviya, "Optimization Techniques Used in Machining Processes: A Review," in *Recent Advances in Materials and Manufacturing Technology*, Singapore, R. K. Nayak, M. K. Pradhan, A. Mandal, and J. P. Davim, Eds., 2023: Springer Nature Singapore, pp. 93-101.
- [18] E. M. Gutema, M. Gopal, and H. G. Lemu, "Minimization of Surface Roughness and Temperature during Turning of Aluminum 6061 Using Response Surface Methodology and Desirability Function Analysis," *Materials*, vol. 15, no. 21, p. 7638, 2022.
- [19] J. H. Shaik and S. J., "Optimal selection of operating parameters in end milling of Al-6061 work materials using multi-objective approach," *Mechanics of Advanced Materials and Modern Processes*, vol. 3, no. 1, p. 5, 2017.
- [20] D. B. Niranjan, G. S. Shivashankar, K. V. Sreenivas Rao, and R. Praveen, "Optimization of Cutting Process Parameters on AL6061 Using ANOVA and TAGUCHI Method," *Materials Today: Proceedings*, vol. 4, no. 10, pp. 10845-10849, 2017.
- [21] W. S. Miller, L. Zhuang, J. Bottema, A. J. Wittebrood, P. De Smet, A. Haszler, and A. Vieregge, "Recent development in aluminium alloys for the automotive industry," *Materials Science and Engineering: A*, vol. 280, no. 1, pp. 37-49, 2000.
- [22] Ö. Seçgin and M. Z. Sogut, "Surface roughness optimization in milling operation for aluminum alloy (Al 6061-T6) in aviation manufacturing elements," *Aircraft Engineering and Aerospace Technology*, vol. 93, no. 8, pp. 1367-1374, 2021.
- [23] S. R. Zaidi, N. Ul Qadir, S. H. I. Jaffery, M. A. Khan, M. Khan, and J. Petru, "Statistical Analysis of Machining Parameters on Burr Formation, Surface Roughness and Energy Consumption during Milling of Aluminium Alloy Al 6061-T6," *Materials*, vol. 15, no. 22, p. 8065, 2022.
- [24] Y. Bello, S. O. Yakubu, T. N. Guma, and A. S. Imam, "Multi-Response Optimization of Machining Parameters in Turning 6061 Aluminum Alloy Using Grey-Taguchi Approach," *World Scientific News*, vol. 169, pp. 136-151, 2022.
- [25] D. Deepak and B. Rajendra, "Optimization of machining parameters for turning of Al6061 using robust design principle to minimize the surface roughness," *Procedia Technology*, vol. 24, pp. 372-378, 2016.
- [26] M. Javidikia, M. Sadeghifar, V. Songmene, and M. Jahazi, "Analysis and optimization of surface roughness in turning of AA6061-T6 under various environments and parameters," *Procedia CIRP*, vol. 101, pp. 17-20, 2021.
- [27] A. M. Țițu, A. V. Sandu, A. B. Pop, Ș. Țițu, D. N. Frățilă, C. Ceocca, and A. Boroiiu, "Design of experiment in the milling process of aluminum alloys in the aerospace industry," *Applied Sciences*, vol. 10, no. 19, p. 6951, 2020.
- [28] Y. Fu, Y. Zhou, Z. Yang, and J. Yang, "Evaluation on the performance of hybrid textured coated tool under conventional cooling environment," *Surface Topography: Metrology and Properties*, vol. 9, no. 4, p. 045011, 2021.
- [29] X. Hua, J. Caesar Puoza, J. Sun, P. Zhang, J. Ji, H. Wang, H. Fu, and Z. Kang, "Experimental analysis of friction and wear of laser microtextured surface filled with composite solid lubricant and lubricated with grease on sliding surfaces," *Journal of Tribology*, vol. 139, no. 2, p. 021609, 2017.
- [30] M. Kuntoğlu, A. Aslan, D. Y. Pimenov, K. Giasin, T. Mikolajczyk, and S. Sharma, "Modeling of Cutting Parameters and Tool Geometry for Multi-Criteria Optimization of Surface Roughness and Vibration via Response Surface Methodology in Turning of AISI 5140 Steel," (in eng), *Materials (Basel)*, vol. 13, no. 19, 2020.